NBSIR 74-486

Reliability, Life Prediction and Proof Testing of Ceramics

S. M. Wiederhorn

Inorganic Materials Division
Institute for Materials Research
National Bureau of Standards
Washington, D.C. 20234

May 1974

Interim Report for Period July 1, 1973 through June 30, 1974

Prepared for

Department of the Navy
Office of Naval Research
Arlington, Virginia 22217

NBSIR 74-486

RELIABILITY, LIFE PREDICTION AND PROOF TESTING OF CERAMICS

S. M. Wiederhorn

Inorganic Materials Division
Institute for Materials Research
National Bureau of Standards
Washington, D.C. 20234

May 1974

Interim Report for Period July 1, 1973 through June 30, 1974

To be published in Proceedings of Conference, "Ceramics for High Performance Applications," Hyannis, Mass., Nov. 13-16, 1973.

Prepared for
Department of the Navy
Office of Naval Research
Arlington, Virginia 22217

U. S. DEPARTMENT OF COMMERCE, Frederick B. Dent, Secretary

NATIONAL BUREAU OF STANDARDS, Richard W. Roberts, Director

RELIABILITY, LIFE PREDICTION AND PROOF TESTING OF CERAMICS

By

S. M. Wiederhorn
Institute for Materials Research
National Bureau of Standards
Washington, D.C. 20234

Abstract

A critical review is presented of the use of proof testing as a design method for assuring the reliability of structural components. The advantage of proof testing over the statistical approach used for design lies in the insensitivity of the proof testing method to the detailed history of handling or processing of structural components. Methods are presented for developing and using proof test diagrams to assure component lifetime after proof testing. Procedures of proof testing and precautions that must be followed during proof testing are discussed. Provided these precautions are followed, proof testing offers a general method for assuring the reliability of structural components under stress.

1. Introduction

Because of its value as a method of assuring structural reliability, proof testing is often used in the design of structural ceramics. Proof testing is especially valuable in applications in which ceramics are subjected to tensile stresses. In proof testing, ceramic components are subjected to stresses that are greater than those expected in service in order to break the weak components and thus to truncate the low end of the strength distribution. In this manner, weak components are eliminated before they can be placed in service. Proof testing has been applied to windows for spacecraft and experimental aircraft,[1-3] to electrical porcelain insulators that are expected to support tensile loads for long periods of time,[4] and to ceramic pressure vessels.[5] Proof testing also finds application in more complex situations in which complete engineering assemblies are tested. In this way, proof testing is used to assure the performance of aircraft engines and may find similar application in gas turbines for energy generation.

Despite its great value for assuring reliability, proof testing has had no firm theoretical basis until very recently. Using trial-and-error estimates, proof test loads for ceramic materials were generally set at two to six times the expected load. Whereas such estimates have usually resulted in reliable structural ceramics, a more systematic method of

selecting a proof test load offers the advantage of either lighter structural components or fewer rejects due to breakage during the proof test. A more systematic method of selecting a proof test load also eliminates the possibility of selecting a test load too small to assure structural reliability. We gain these advantages because a more exact value of the proof test load can be selected for a given application.

Recognizing the need for greater insight into proof testing, Wiederhorn, Evans and Fuller[6-9] provided a mathematical foundation for the selection of the proof test load and for the establishment of proof test conditions. Their analysis is based on the fact that failure of ceramic materials occurs mainly from the growth of preexisting cracks. By characterizing crack growth, and coupling crack growth parameters with proof testing, they have demonstrated how to construct design diagrams that relate the expected failure time to the maximum design stress. Their analysis provides a rational guide for the selection of both proof test load and test conditions. Since these are the keys to a successful proof test, the analysis by Wiederhorn, Evans and Fuller is the basis of a general method that can be incorporated into the design of structural ceramics.

This paper presents a review of the mathematical foundation for proof testing. For clarity of presentation, most of the important equations are derived from first principles. Examples are given of how

these equations may be used to assure structural reliability. The proof testing technique is compared with the technique of structural design that is based on Weibull statistics, and the superiority of the proof testing technique is demonstrated.

In developing the mathematical foundation of proof testing, an estimate is first presented of the time to failure due to crack growth. The time to failure is shown to depend critically on the size of the largest flaw contained within the structural component. By using a proof test method, or a statistical analysis of strength to estimate the critical flaw size, design diagrams are obtained that relate the failure time to the service stress. The value of proof testing ceramic components prior to use is discussed and precautions are presented for conducting proof tests on brittle materials. It is hoped that this paper will provide the background needed to develop better design techniques for structural ceramic materials.

2. FAILURE TIME UNDER STRESS

The time required for the failure of a ceramic component under tensile stress can be calculated by using fracture mechanics concepts. For most materials, the stress intensity factor, K_I, at a flaw is related to the applied stress, σ_a, and flaw size, a, by the following equation:

$$K_I = \sigma_a Y\sqrt{a} \tag{1}$$

Y in the above equation is a geometric constant that depends on both the shape and location of the flaw, and the type of stress applied to the material.[10] For surface flaws (cracks) which are usually the most critical flaws in ceramic materials, $Y \simeq \sqrt{\pi}$. For a constant applied stress the derivative of both sides of Eq. (1) with respect to time yields the following equation, where v is the crack velocity,

$$dK_I/dt = (\sigma_a^2 Y^2/2K_I)v \tag{2}$$

By separating the variables of Eq. (2) and rearranging the equation, the following expression is obtained for the total time-to-failure under constant load, where K_{IC} is the critical stress intensity factor and K_{Ii} is the initial stress intensity factor at the most serious flaw in the component.

$$t = (2/\sigma_a^2 Y^2) \int_{K_{Ii}}^{K_{IC}} (K_I/v) dK_I \tag{3}$$

Evaluation of Eq. (3) requires information on the critical stress intensity factor, the initial stress intensity factor at the most serious flaw, and the functional relationship between the stress intensity factor and the crack velocity. The critical stress intensity factor is obtained by fracture mechanics techniques. Fracture mechanics specimens are broken in an inert environment and K_{IC} is calculated from the dimensions of the specimen, the crack length, and the failure load. A critical review

of techniques commonly used to determine K_{IC} on ceramic components may be found in Ref. 11.

The relationship between the stress intensity factor and the crack velocity in a given environment can also be found by fracture mechanics techniques. Usually crack velocity measurements are made on specimens similar in shape and size to those used for critical stress intensity factor measurements. Again, the stress intensity factor is calculated from the crack length, load and specimen dimensions. Although fracture mechanics techniques are commonly used to collect crack growth data, these data can also be obtained by measuring the strength as a function of loading rate. A critical review of these methods has been presented in Ref. 12. For the purposes of the present paper, it should be recognized that both the critical stress intensity factor and the relationship between the crack velocity and the applied stress intensity factor are easy to measure.

For many ceramic materials, the crack velocity is a power function of the stress intensity factor, $v = AK_I^n$, in which case Eq. (3) is integrated to give (to a good approximation) the following equation for the time to failure:

$$t = 2K_{Ii}^{2-n}/A\sigma_a^2 Y^2 (n-2) \qquad (4)$$

However, other analytical expressions relating K_I to v may also be used, or if no simple expression is available, Eq. (3) can be integrated numerically.

Because of its dependence on flaw size, K_{Ii} in Eqs. (3) and (4) is not easily measured on real components. Flaws in most ceramic materials are less than 1 mm in size and their dimensions are not easily measured by nondestructive means.* Therefore, indirect methods must be used to estimate the size of flaws in ceramic materials.

There are two indirect methods for determining the initial size of the most serious flaw in ceramic materials. One method uses statistics to characterize the strength of the ceramic component as a function of the cumulative probability for failure. The flaw size is then estimated on a statistical basis by substituting the results of the statistical analysis into Eq. (1). The second method employs a proof test to determine the maximum size flaw in the component at the time of the test. Once an estimate of a_i is available (by either method) the initial stress intensity factor is determined from the equation: $K_{Ii} = \sigma_a Y\sqrt{a_i}$. The expected service life of the component can then be calculated by substituting K_{Ii} into Eq. (3) or (4).

3. STATISTICAL APPROACH

The statistical approach usually used to describe the strength of materials was originally developed by Weibull.[13] This technique uses a form of extreme value statistics that is particularly sensitive to the

---

*By contrast, flaws in metals are larger and can be measured by a variety of nondestructive techniques: X-ray radiography, ultrasonics, dye penetrants, etc.

low strength end of the strength distribution. Weibull's relationship between the cumulative failure probability*, P, and the strength σ_{IC} is given by the following equation:

$$P = 1 - \exp -[(\sigma_{IC} - \sigma_{\ell})/\sigma_o]^m \qquad (5)$$

where σ_o, σ_{ℓ}, and m are empirical constants. σ_{IC} is the strength measured under the condition that no subcritical crack growth occurs prior to failure, and should be determined in an inert environment using rapid loading rates. By arranging the strength measurements in order of increasing strength, P may be determined from the equation: $P = j/(J + 1)$, where j is the position of the jth strength measurement in the ordered set of strengths and J is the total number of measurements. σ_{ℓ}, the lowest possible strength, is usually set equal to zero. σ_o is a scaling parameter and m is a shape parameter. m and σ_o are determined by fitting a straight line to the strength data which have been plotted as log log $(1/1 - P)$ versus log σ_{IC} (Fig. 1); the slope of the line is m whereas the intercept is m log σ_o.

In practice the Weibull theory is easy to apply because once m and σ_o have been evaluated the strength is uniquely characterized on a statistical basis. However, some precautions must be exercised when the Weibull theory is used for strength analysis. m and σ_o may vary from one component to the next due to the susceptibility of strength to variations in the manufacturing process. Because of these variations, m and σ_o determined on laboratory specimens may not be correct for

---

*The cumulative failure probability gives the fraction of specimens that will break at a given stress level.

structural components. m and σ_o are also subject to inaccuracies which result from the statistical uncertainty encountered whenever a straight line is fitted to a set of experimental data. If only a small number of strength measurements are used to determine m and σ_o, the statistical uncertainty of these parameters can cause substantial errors in estimates of the strength at low failure probability. As shown in Fig. 1 this uncertainty in strength increases as the failure probability decreases. Finally, even if σ_o and m are accurately determined, errors in estimating the strength may occur because strength depends on component size. Because of the greater probability of larger flaws, large components are usually weaker than small ones. Although scaling equations are used to account for size effects, these equations are sometimes difficult to obtain and may be complex, especially for complex stress distributions. Furthermore the location of the flaw that causes failure must be identified, because scaling equations differ depending on whether the crucial flaws lie at the surface or in the volume of the component. Because of uncertain information regarding the flaw location, scaling equations must be tested for accuracy by using laboratory test specimens of varying size and shape. All of these considerations decrease the value of Weibull statistics as a method of determining strength. Consequently, design values of strength must be more conservative than those given by equation 5.

Although the method used by Weibull did not consider strength as a time dependent variable, a time dependence due to crack growth can be

easily introduced into the Weibull method by expressing K_{Ii} in terms of the failure probability.[7,14] At failure, the critical stress intensity factor, K_{IC}, the fracture strength, σ_{IC}, and the crack length, a_i, are related by: $K_{IC} = \sigma_{IC} Y\sqrt{a_i}$. At the service load the initial stress intensity factor, K_{Ii}, is related to the service stress, σ_a, and the crack length by: $K_{Ii} = \sigma_a Y\sqrt{a_i}$. From these two equations, an equation for K_{Ii} is obtained:

$$K_{Ii} = K_{IC}(\sigma_a/\sigma_{IC}) \tag{6}$$

By substituting Eq. (5) (with $\sigma_\ell = o$) into this equation, an equation may be obtained relating K_{Ii} to the cumulative failure probability:

$$K_{Ii} = K_{IC}(\sigma_a/\sigma_o)\ [\log(1/1 - P)]^{-1/m} \tag{7}$$

This equation may now be substituted into Eq. (3) or (4) to obtain an equation that relates the failure time to the cumulative probability for failure. The functional form of this equation is:

$$t = \sigma_a^{-n} \cdot f(P) \tag{8}$$

For each value of P the failure time is a power function of the applied stress. Therefore a series of straight lines of slope -n can be

obtained from a logarithmic plot of t versus σ_a (Fig. 2), each line representing a different value of P. This type of diagram completely describes the failure characteristics of a material on a statistical basis. Similar diagrams are often used to represent static fatigue data. However their value is more limited for design purposes because only the average or median strength is used as a plotting parameter. By contrast, diagrams such as that given in Fig. 2 represent the general fatigue behavior of a material and are more useful for design purposes.

To illustrate how the diagram can be used for design purposes, refer to the data of Fig. 2 which was obtained on a glass that is being considered for the space shuttle.[3] During its lifetime the shuttle will undergo many stress cycles. The windows must not fracture during the critical period of each cycle when the spacecraft is in orbit. To assure reliable performance, the windows should be able to survive for at least one year under load while subjected to the most severe environmental conditions expected in each cycle. Since the spacecraft will be periodically exposed to moist air, and since water causes stress corrosion in glass, the most adverse environment for the proposed space shuttle glass would be a moist environment. For this reason, the diagram shown in Fig. 2 has been based on crack propagation data collected on glass specimens that were immersed in water. From Fig. 2 we see that for a failure probability of 10^{-5} the windows can be subjected to a stress of no more than 2,000 psi if one year's survival is desired. This stress value is approximately one-half the present design load, 4,000 psi. If

a design load of 4,000 psi is used the probability of failure for these windows increases to approximately 2×10^{-3}, a probability much too high for safety. Hence, we see that the statistical approach leads to low design values of the load if low failure probabilities are required.

The design load suggested from Fig. 2 has not been scaled for the fact that laboratory specimens were much smaller than the spacecraft windows. The laboratory specimens used to evaluate m and σ_o were disks approximately one inch in diameter, while spacecraft windows will be trapezoids approximately 1000 in^2. If the high stress regions of these two sets of specimens are assumed to be proportional to their areas, then to a first order approximation the Weibull approach predicts a reduction of strength proportional to the ratio of the two areas raised to the 1/m power, which reduces the strength of glass by a factor of 3 for all probability levels. This reduction limits the use at the 10^{-5} probability level to a strength of approximately 700 psi instead of the 2000 psi shown in Fig. 2. A further reduction in stress may be required because of uncertainties in the assumption of equal distribution of flaws in large and small components and because of the very simplified treatment used to get the correction ratio.

4. PROOF TESTING APPROACH

Proof testing removes many of the difficulties present in the statistical approach to failure. Proof testing truncates the strength distribution, eliminating those specimens with the largest probability for failure.* As a result, components can be used at higher stress levels with greater assurance of reliability than can be obtained from the statistical approach.

---

*For effective proof testing, all components intended for service must be tested.

To develop the mathematical basis for proof testing, one must recognize that a proof test limits the maximum flaw size that can be present in the specimen after the proof test.*[15] All specimens containing flaws larger than this critical value will fail during the proof test, because the stress intensity factor at the tips of the flaws will exceed the critical stress intensity factor, K_{IC}. For flaws that are smaller than the critical size, the stress intensity factor will be less than the critical stress intensity factor and the components will survive the proof test. Therefore, if failure does not occur during a proof test, $K_{IC} > K_P = \sigma_P Y\sqrt{a_i}$, where K_P is the stress intensity factor at the largest flaw during the proof test, and σ_P is the stress applied during the proof test. When the component is first used in service, the relationship between the initial stress intensity factor, K_{Ii}, the applied stress, σ_a, and the flaw size is given by $K_{Ii} = \sigma_a Y\sqrt{a_i}$. From these two equations, the following equation is obtained:

$$K_{Ii} < K_{IC}(\sigma_a/\sigma_P) \tag{9}$$

This estimate for the initial stress intensity factor can be substituted into Eq. (3) or (4) to obtain an estimate for the minimum time to failure. Because the limits of integration of Eq. (3) depend only on the ratio of the proof test load to the applied load, the minimum time to failure, t_{min}, is given by the following functional relationship:

---

*In this section it is assumed that crack growth does not occur during the proof test. Crack growth during the proof test is discussed in section 5.4.

$$t_{min} = \sigma_a^{-2} \cdot f(\sigma_p/\sigma_a) \qquad (10)$$

Thus, for any given proof test ratio, σ_p/σ_a, the minimum time to failure is inversely proportional to the square of the applied stress. A logarithmic plot of the minimum time to failure versus the applied stress gives a straight line with a slope of -2, the position of the straight line depending on the proof test ratio.

A design diagram incorporating these ideas is presented in Fig. 3, which is a logarithmic plot of the time to failure versus the applied stress. Lines derived from the statistical approach to failure are also included in this diagram for comparison. For a survival time of one year at a stress of 4000 psi, a proof test ratio of 2.6 will be necessary for this glass. Specimens passing the proof test will survive the minimum time to failure with zero probability of earlier failure. By comparison, the failure probability is 2×10^{-3} at the same stress levels in the absence of a proof test. To pass the proof test, the glass windows will have to sustain a load of approximately 11,000 psi.

Referring now to the Weibull diagram for these glasses (Fig. 1), it is observed that at a stress level of 11,000 psi only one specimen in a thousand will be broken during the proof test. If the reduction in strength is taken into account because the glass windows are much larger than the disks tested in this experiment, a failure rate of one in ten is reached. Thus, by taking the chance that one window out of ten will break during the proof test, adequate performance of the remaining windows is assured.

As shown in an analysis by Evans and Fuller, proof testing can also be applied to cyclic loading.[8] If failure involves subcritical crack growth, the failure time due to cyclic loading, t_c, is proportional to the failure time, t_{min}, due to static loading: $t_c = g^{-1} t_{min}$, where g^{-1} is a proportionality constant that can be evaluated by a numerical integration for any periodic load cycle. For square wave, sinusoidal or saw-tooth type of loading, values of g^{-1} have been evaluated analytically and are available in diagrams that express g^{-1} as a function of the exponent n and the ratio σ_1/σ_a, where σ_1 is the stress amplitude and σ_a is the average applied stress. (Fig. 4). t_{min} is determined from a design diagram (Fig. 3) by setting the service stress equal to the average applied stress for the cycle. The analysis by Evans and Fuller permits a direct comparison of experimentally determined crack growth data and failure times for cyclic and static loads. Agreement between these two types of data indicates that failure is most likely due to subcritical crack growth. However if these two types of data do not agree, failure is most likely the result of some mechanism besides subcritical crack growth due to static loading. Crack propagation and strength results on porcelain, alumina and glass at room temperature[8] and on silicon nitride and alumina at high temperature,[16] give no indication of an enhanced effect of cyclic loading on slow crack growth. Consequently, by using g^{-1}, design diagrams developed for failure predictions for static loading are also applicable to cyclic loading of these materials.

The main advantage of the proof test procedure is its relative insensitivity to the particular flaw distribution associated with a given component. Since the flaw size distribution is determined by the component's history, it follows that the proof test method of assuring reliability is independent of the component's history prior to the time of the test. By contrast, diagrams obtained from statistical considerations are extremely sensitive to the flaw size distribution and therefore to the component's history. A further advantage of the proof test method is its insensitivity to the particular arrangement of flaws in a component. Thus even though the analysis of failure assumes that the most serious flaw lies perpendicular to the maximum stress, a deviation from this condition leads to a more conservative estimate of failure time.[6]

5. PRECAUTIONS IN PROOF TESTING

In this section a discussion is presented of some of the precautions to be exercised when proof testing is used for design. These precautions are concerned with the service stresses, the accuracy and applicability of the crack growth data, the design of proper proof test procedures and the possibility of strength degradation as a consequence of the proof test. This discussion is necessary since an incorrect assessment of any of these precautions could invalidate the proof test and result in premature component failure.

5.1 Stress Equivalence During Proof Testing

Proof testing is based on the assumption that all parts of a structural component are subjected to the required proof stresses during the proof test. At any point in the component these stresses must exceed the

service stresses by a specified amount, otherwise portions of the component will remain untested and predictions of component lifetime will not be meaningful. Therefore proof tests must duplicate the expected service stress distribution as closely as possible. For simple components such as windows for pressure vessels or electrical porcelain suspension insulators, service stresses are easily duplicated by applying loads that exceed the service load by the required amount. However, for other types of components duplication of the service stress distribution may be more difficult because of complicated component geometry or stress distribution. In some cases a double proof test may be necessary to test different types of loading expected in service. For example, proof tests for turbine rotors must duplicate the stresses resulting from both the centrifugal force and the gas pressure on the vanes of the rotor. In general, each structural component must be considered individually to decide on the appropriate proof test.

5.2 Parasitic Stresses

The results of a proof test are sometimes invalidated by parasitic stresses that cause strength deterioration or crack growth over and above that predicted by the proof test. Parasitic stresses arise from unintended features of the proof test, for example, if the proof test apparatus inadvertently applies loads that differ from the service loads. An example of component deterioration due to parasitic stresses was recently observed in large porcelain insulators meant to support radio towers.[4] The proof test

consisted of slowly increasing the load on the insulators to 2.5 x 10^6 pounds, and then slowly decreasing it to zero load. During the proof test,acoustic emission transducers that were attached to the insulator indicated high rates of emission at approximately two million pounds as the load on the insulator was decreasing. The emission was due to the growth of a large internal crack during the unloading procedure.* The presence of this crack was confirmed by an ultrasonic examination of the insulator during the test. The stresses that caused the crack to grow resulted from unexpected slippage of the porcelain in its metallic end caps.** As a consequence of this observation, it may be concluded that proof test procedures should be designed to avoid parasitic stresses.

5.3 Equivalence of Crack Propagation Data and Failure Mechanism

The proof test method of assuring reliability depends critically on an accurate evaluation of the crack propagation parameters that control fracture. If proof test methods are to be of value, these parameters must represent the failure mechanism. Therefore, information on the factors that determine the crack propagation parameters is essential. These factors include: the crack tip environment; the size of the strength limiting flaw relative to the microstructure of the component; and the functional dependence of crack velocity on stress intensity factor.

---

*The crack growth detected by acoustic emission transducers does not necessarily result in mechanical failure for compressive loading. These porcelain insulators are not acceptable for service if they contain large cracks because the cracks cause the insulators to become electrically unstable.

**We suspect that this type of failure may be characteristic of some kinds of compressive loading.

For many materials (ceramics, metals and polymers) environment is the dominant factor that controls crack growth. Many structural ceramics are sensitive to water in the environment, which causes stress corrosion cracking.[12] As water penetrates to the crack tip, crack motion results from a stress enhanced chemical reaction between the water and the material at the crack tip. This reaction can occur even in relatively dry gases[17] or in organic liquids[18]. In aqueous solutions the reaction is sensitive to the pH of the solution.[19] In glass for example crack propagation curves are steeper in high pH solutions than in low pH solutions[3,19] (Fig. 5). Finally, the crack tip environment may differ from the bulk environment as a result of the chemical reaction at the crack tip.[19] Therefore, to use crack propagation data for failure prediction purposes, one has to be certain that the crack tip environment is the same for the crack propagation measurements as for the component in service.

Another factor that influences the crack growth is the size of the strength limiting flaws relative to features of the microstructure such as grain size, pore size, or pore spacing. The relative flaw size is important because of a possible dependence of crack propagation rate on microstructure. In crack growth studies, the flaw is artificially produced and is always larger than characteristic dimensions of the microstructure. However in some materials, the flaws that limit strength are comparable in size to the microstructure. Therefore, crack growth behavior of these flaws will not necessarily be described by crack growth data obtained on fracture mechanics specimens. As a consequence,

failure predictions may not be valid if they are based only on design diagrams derived from this growth data. Fortunately, for many materials the flaw size is large relative to the microstructure and the assumptions used to construct proof test diagrams are valid. In hot-pressed silicon nitride for example the flaw size, 100μm, is approximately 100 times the grain size.[20] Similarly, cracks in glass are usually much larger than the inhomogeneities that may be present in this material. This assumption of large crack size is not valid for other materials. For example, the crack size in aluminum oxide is approximately equal to the grain size.[21] For these materials, proof test diagrams should be used only if it can be shown on a laboratory scale that material strength can be predicted from these diagrams. Agreement between strength measurements and crack propagation data in laboratory studies would permit these diagrams to be used for design purposes.

The functional dependence of crack velocity on stress intensity factor is another variable that must be considered in the design of a proof test. Knowledge of this functional dependence is important when large values of the proof test ratio are used for design. In this case the crack propagation data have to be extrapolated to low values of the velocity, and the accuracy of the extrapolation determines the validity of the time-to-failure prediction. This point is illustrated in Fig. 6 which gives a logarithmic plot of $f(\sigma_p/\sigma_a)$ from Eq. (10) versus σ_p/σ_a for two representations of the crack velocity data, (a logarithmic and a power function representation). As $f(\sigma_p/\sigma_a)$ and σ_p/σ_a exceed the limits

of the experimental data, given by the cross in the figure, the two curves diverge, resulting in some uncertainty in the selection of an appropriate proof test ratio. For the proposed space shuttle glass this uncertainty was not large since the power function representation of Fig. 6 suggested a proof test ratio of 2.6 to 1 for a year's lifetime at 4,000 psi, while the exponential representation suggested a proof test ratio of just over 2.8 to 1 for the same stress. However, for other materials this uncertainty might be crucial. To avoid this source of error, crack velocity data should be collected at as low a velocity as is feasible.*

One way to assure the applicability of crack growth data to failure predictions is to demonstrate an agreement between the strength and crack growth data. This agreement has been demonstrated for the glass proposed for the space shuttle[3] (Fig. 7) and for hot pressed silicon nitride[22] (Fig. 8). The points in Fig. 7 represent the mean value of the strength of the space shuttle glass obtained for each value of the loading rate; the brackets give 95 percent confidence limits for the mean values. The solid straight line is a least squares fit of all of the strength data, while the dashed line is the predicted strength from crack propagation data. Since the dashed line falls within the 95 percent confidence limits of the strength data, one may conclude that for this glass the crack propagation data and the proof test diagram

*Since approximately one month is required to measure a crack velocity of 10^{-11} meters per second, this velocity appears to represent a lower practical limit for crack propagation data.

derived from it can be used effectively for design purposes. Similar agreement is found for the silicon nitride data given in Fig. 8 where a comparison is presented between strength data obtained at 1400° C[23] and crack propagation data (the solid lines) obtained at the same temperature.[22] The lines fall close to the measured strength values suggesting that crack propagation data on hot pressed silicon nitride gives adequate predictions of strength, and that proof test diagrams can be used for design purposes for this material.

For general application of the proof test method, additional comparisons between crack propagation data and strength data will be necessary. An equivalence between crack propagation data and strength data should be demonstrated on a laboratory scale for each material so that proof test diagrams can be used confidently for design purposes.

5.4 Loading Procedure During Proof Test

In section 4 the minimum time to failure, t_{min}, was estimated on the assumption that crack growth did not occur during the proof test. In addition, failure was assumed to occur instantaneously if the critical stress intensity factor was exceeded at some flaw in the component. As a consequence of these assumptions, the failure probability was found to be zero for all periods of time that were less than the minimum failure time, t_{min}. While these assumptions are valid for some commercially important materials (silicon nitride and silicon carbide tested in air at room temperature;[24] silica, chemical Pyrex and the space shuttle glass tested

in vacuum[25]), they are not valid for others. Soda lime silicate type glasses, for example, exhibit subcritical crack growth even in a vacuum.[25] If crack growth occurs during a proof test, then the failure probability is no longer zero, but has a finite value that is determined by the proof test conditions and the test environment. Fortunately, the failure probability can be reduced to a vanishingly small quantity by judicious selection of the proof test conditions.

A theoretical basis for selection of the proof test conditions has been developed recently by Evans and Fuller[9] who have examined the effect of crack growth on the failure probability after proof testing.* Evans and Fuller assumedthat constant rates of loading, $\dot{\sigma}_\ell$, and unloading, $\dot{\sigma}_u$, were used in the proof test, and that the proof test load, σ_p, was held on the component for a period of time, t_p. They also assumed that crack growth was controlled by a single fracture mechanism so that the crack growth rate could be expressed as a power function of the stress intensity factor, $v = AK_I^n$. Using these assumptions, they found that the crack length after a proof test could be described by the following equation:

$$a = a_o\left[1 - (a_o/a_o^*)^{\frac{n-2}{2}}\right]^{\frac{-2}{n-2}} \qquad (11)$$

---

*Their theory is fully developed in the appendix for the interested reader.

where a is the crack length after completion of the proof test and a_o is the initial crack length. a_o^*, the critical crack length for failure during the proof test, is the initial length of a crack that will just grow to failure during the proof test. As shown by the following equation a_o^* is completely determined by the proof test conditions:

$$a_o^* = \{[(A\sigma_p^n Y^n (n-2)/2][(t_p + (t_\ell + t_u)/(n+1)]\}^{\frac{-2}{n-2}} \qquad (12)$$

where $t_\ell = \sigma_p/\dot{\sigma}_\ell$ is the time required to load the component to the proof test load, σ_p, and $t_u = \sigma_p/\dot{\sigma}_u$ is the time required to unload the component.

The dependence of crack length a on a_o is depicted in Fig. 9 for n = 20 and n = 100. As indicated by the abrupt increase in a/a_o as a_o approaches a_o^*, crack growth is significant only when a_o is close in value to a_o^*. Because of this behavior, strength degradation is serious only for components that contain cracks for which $a_o \tilde{-} a_o^*$.

The failure probability after a proof test is determined by the range of initial crack lengths that result in significant crack growth (R of Fig. 9): The narrower the range of the crack lengths, the lower the failure probability. Since this range is small for large values of n, test environments should be selected so that n is large. Thus, proof tests on soda lime silicate glass should be conducted in dry nitrogen for which $n \tilde{-} 100$ rather than in air for which $n \tilde{-} 20$. This conclusion is supported by a detailed calculation of the failure probability after a proof test.

An estimate of the probability for failure after a proof test can be obtained by using the crack length, a, of equation 11 to evaluate K_{Ii} of Eq. (4). After rearranging the equation and using a Weibull analysis to describe the initial crack size distribution (see appendix), the following equation is obtained for the failure probability, P_a, after a proof test:

$$P_a = \frac{m}{n-2} (\sigma_P/\sigma_o)^m (K_P^*/K_{IC})^{n-m-2} (t/t_{min})^{\frac{n-2}{n^*-2}} \quad (13)$$

where: m and σ_o are Weibull parameters; n and n^* are crack propagation equation exponents, n referring to the test environment and n^* referring to the service environment; and t_{min} is the minimum failure time calculated from Fig. 3 which is based on the assumption that crack growth does not occur during the proof test. t is the time in service after the proof test. K_P^* is the stress intensity factor calculated for a crack of length a_o^*; $K_P^* = \sigma_P Y\sqrt{a_o^*}$. K_P^* would be the stress intensity factor for this crack if crack growth did not occur during the proof test.

P_a is a useful engineering quantity because it gives the fraction of components that break in service in a period of time t. P_a is a function of the time at load, increasing with service time, t. By a proper selection of the proof test procedure, P_a, can in principle be made arbitrarily small. Since n is usually much larger than n^*, the failure probability is very sensitive to the ratio t/t_{min}. Therefore by selecting the service time to be less than t_{min}, the value of P_a can be reduced without limit. In practice this

requires the proof test load to be increased over the value estimated if crack growth did not occur during the proof test. This increase of proof test load is usually not excessive for $t/t_{min} \tilde{-} 0.1$.

K_P^* is completely determined by the proof test conditions and can be evaluated from the following equation which relates the crack propagation data to the proof test conditions:

$$(K_P^*)^2/v_P = [\sigma_P^2 Y^2 (n-2)/2]\ [t_P + (t_\ell + t_u)/(n+1)] \qquad (14)$$

The right hand side of this equation (14) is easily evaluated from the proof test load, σ_P, the crack propagation parameter, n, the loading and unloading times, t_ℓ and t_u, and the time, t_P, that the component is exposed to the proof test load. To evaluate K_P^* from the above equation, a plot of K_I^2/v versus K_I is useful, since K_P^* can be easily evaluated from such a diagram once $(K_P^*)^2/v_P$ has been determined from Eq. 14.*

The use of Eq. (13) will now be demonstrated for abraded soda lime silicate glass, for which a Weibull plot is given in Fig.10 and the crack propagation data is given in Fig. 11. A plot of K_I^2/v versus K_I calculated from the crack propagation data is given in Fig. 12. For illustrative purposes suppose that the glass is required to support a load of 4 MN/m^2 (~570 psi) for a period of 10^5 seconds in a wet environment. By selecting t_{min} to be 10^6 seconds a proof test ratio of 3 is

---

*$v_P \equiv A(K_P^*)^n$.

estimated from Fig. 13; thus σ_P = 12 MN/m^2. This proof test ratio is larger than the ratio of 2.6 that would be required if crack growth did not occur during the proof test. If the proof test is conducted in a moisture-free environment, n $\simeq$ 100 while $n^* \simeq$ 20. K_{IC} for soda lime silicate glass[26] is 0.75 MN/m$^{3/2}$ and from Fig. 10 m = 2.63 and σ_o = 45 MN/m^2. If the glass components are loaded and unloaded in a relatively short time, ~10 sec, and if the proof load is applied for ~1 sec, then from Eq. (14) $(K_P^*)^2/v_P$ is calculated to be 2.66 x 10^{16}. From the vacuum curve in Fig. 12, K_P^* is estimated to be 0.71 MN/M$^{3/2}$. By substituting these values into Eq. 13 a value of 1.6 x 10^{-11} is obtained for P_a, which for practical purposes is equal to zero. The fraction of specimens that would have been broken in the proof test, given by $P_P = (\sigma_P K_{IC}/\sigma_o K_P^*)^m$ (see appendix), is 0.03. If the glass had been used without prior proof testing the failure probability from Fig. 13 would have been approximately 5 x 10^{-3} at the service conditions (σ_a = 4 MN/m^2; t = 10^5 sec). Thus by breaking only 3 percent of the components during the proof test, a much greater assurance of reliability is obtained.

The assurance of reliability is not nearly as great if the proof test is conducted in a wet environment, for which $n = n^* = 20$. For the same loading conditions and proof load, $(K_P^*)^2/v_P$ is 7.95 x 10^{15}, and K_P^* calculated from Fig. 11 (the curve for water) is 0.58 MN/m^2. P_a is now 8.7 x 10^{-5} and the fraction breaking during the proof test is approximately 0.061. Although the failure probability in a wet environment can be improved

by increasing K_p^2/v_p (by increasing t_p for example) the values are never as small as those obtained in a dry environment using the same test conditions. Thus, whenever possible, inert environments should be used for proof tests.

From the above results one may conclude that proof testing is a valuable method of assuring the reliability of structural ceramics even if crack growth occurs during the proof test. To apply the method, a statistical description of the component strength and crack propagation data in both an active and inert environment are needed. However, these types of data are easy to obtain, and once these data have been obtained, they may be used to establish proof test conditions that assure a low failure probability after proof testing.

5.5 Protection of Components after Proof Testing

Although proof testing assures a minimum lifetime at the time of the test, it loses value if subsequent damage occurs. This can be a serious problem for materials which fail from surface flaws, since these flaws are easily introduced into the material by rough handling. This problem can also arise in materials that fail primarily from internal flaws if the structure changes in service. Therefore some considerations have to be given to protection of components after the proof test and to periodic retesting of components during use.

For components that fail from surface flaws, caution in handling or the adoption of some protective measure after proof testing is necessary to assure reliability during service. For glass, which is particularly

susceptible to surface damage, this means that the surfaces have to be protected, perhaps by plastic coatings which would prevent abrasive damage of the surface after proof testing. In the space shuttle windows, damage after proof testing is avoided by the design of the windows. These are triple paned, the tensile stress surfaces being on the interior of the panes. Thus further surface damage by handling cannot occur.

The possibility of strength degradation in service due to the initiation of new flaws must also be considered. This degradation could occur by chemical reactions within the material, by phase transformations, or by pore growth at high temperatures. Strength degradation of this kind is not considered in the equations used to predict the time to failure. Perhaps the best way to eliminate such degradation is by designing the material so that new flaws will not generate during use. However, if this is not possible, periodic proof testing may be needed to assure minimum periods of service life.

6. SUMMARY AND GENERAL CONCLUSIONS

In this paper, proof testing is considered as a general method of assuring reliability of ceramic components for structural uses. A review of current work in this field is presented. The proof test technique is compared with the older statistical approach for design, and it is demonstrated that many of the uncertainties inherent in the statistical approach are eliminated by the use of proof testing. It is shown for example that lifetime predictions after proof testing are not affected by the particular flaw size distribution contained within the specimen, whereas

predictions obtained by the statistical approach are affected by the flaw distribution. In proof testing, predictions of lifetime depend more on material properties, such as the value of the critical stress intensity factor and the relationship between the stress intensity factor and the rate of crack growth in a given environment. Since these both can be determined to high precision, proof test diagrams derived from these parameters should be reliable for the prediction of design lifetimes. However, certain precautions must be exercised in the application of proof testing. The proof test must duplicate the actual stresses expected in the component. Otherwise, the most serious flaw in the specimen might not be subjected to a proof test load. Crack propagation data used to develop design diagrams for proof testing should represent the failure mechanisms that occur in service. To ensure an equivalence between the proof test diagram and the actual failure mechanism, crack propagation data should be compared with data obtained from strength measurements. An agreement between these two types of measurements will lend assurance that the proof test diagram does in fact describe the failure mechanism. The loading procedure during proof test is also important since crack growth during the proof test may result in weak components. To eliminate this problem, the proof test should be conducted in an environment that is relatively inert. An analysis of the loading procedure demonstrates that low probabilities of failure after proof testing can be achieved even if subcritical crack growth does occur during the proof test. The importance of parasitic stresses as a limitation to the proof test method is also discussed. Here it is noted that unexpected stresses may arise during the

proof test. These stresses may in fact damage the specimen to an extent not predicted by the proof test technique. In some cases, the damage may be unavoidable and proof testing may not be a viable procedure. Finally, the necessity of protecting the specimen after proof testing is emphasized since subsequent structural damage may degrade the specimen to a greater extent than is predicted by the proof test. Periodic proof testing is recommended for materials that change structurally or develop damage in service. Provided these precautions are followed, proof testing can be a practical method for assuring the structural reliability of ceramic materials.

Acknowledgment

Portions of this work were supported by the Office of Naval Research, Contract NAonr 5-73, NR032-535.

APPENDIX

PROBABILITY OF FRACTURE AFTER PROOF TESTING

The failure probability after a proof test was calculated by Evans and Fuller[9] by considering the growth of cracks during the proof test. The length to which a crack grows during a proof test can be calculated from the definition of crack velocity, $v = da/dt$, and the functional dependence of crack velocity on stress intensity factor, $v = AK_I^n$. Combining these equations and using the expression $K_I = \sigma(t)Y\sqrt{a}$, the following differential equation is obtained:

$$da/dt = A\sigma^n(t)Y^n a^{n/2} \tag{1A}$$

where the stress, $\sigma(t)$, is a function of time. If the stress, $\sigma(t)$, is known, this equation can be integrated after rearranging the variables. Evans and Fuller assumed that constant stress rates were used to load and unload the component and that the proof stress was held for a time, t_p. The total time to load the components to the proof test load, σ_p, is given by $t_\ell = \sigma_p/\dot{\sigma}_\ell$ where $\dot{\sigma}_\ell$ is the stress rate. Similarly the total time to unload the component is given by $t_u = \sigma_p/\dot{\sigma}_u$. By using these values of time as integration limits, equation (1A) can be integrated to give the following equation for the crack length, a, after the proof test:

$$a = a_o \left[1 - (a_o/a_o^*)^{\frac{n-2}{2}}\right]^{\frac{-2}{n-2}} \tag{2A}$$

where a_o is the crack length before the proof test and a_o^* is the critical crack length that will just result in failure during the proof test. a_o^* is given by the proof test conditions:

$$a_o^* = \{[(A\sigma_p^n Y^n (n-2)/2)][t_p + (t_\ell + t_u)/(n+1)]\}^{\frac{-2}{n-2}} \qquad (3A)$$

Since a is the crack length after the proof test, it is also the initial crack length when the component is placed in service. Therefore, when the component is placed in service, the initial stress intensity factor K_{Ii} is given by: $K_{Ii} = \sigma_a Y\sqrt{a}$. The time to failure after the proof test is given by

$$t = 2K_{Ii}^{2-n^*}/A^*\sigma_a^2 Y^2 (n^*-2) \qquad (4A)$$

Eq. (4A) is identical to Eq. (4) of the text. A^* and n^* represent the crack propagation parameters for an active environment while A and n used in Eqs. (2A) and (3A) represent these parameters in the proof test environment. This distinction is made because the proof test environment may differ from the test environment. By substituting Eq. (2A) and the equation for K_{Ii} into Eq. (4A), the following equation is obtained for the failure time:

$$t = \left[2(\sigma_a Y\sqrt{a_o^*})^{2-n^*}/A^*\sigma_a^2 Y(n^* - 2)\right]\left[(a_o/a_o^*)^{\frac{n-2}{2}} - 1\right]^{\frac{n^*-2}{n-2}} \qquad (5A)$$

By using a_o^* to define a proof test stress intensity factor: $K_P^* = \sigma_P Y\sqrt{a_o^*}$; and by using the identity: $K_P^* = K_{IC}(K_P^*/K_{IC})$, the following equation is obtained for the failure time:

$$t = \left[2(K_{IC}\sigma_a/\sigma_p)^{2-n^*}/A^*\sigma a^2 Y^2 (n^*-2)\right]\left[K_{IC}/K_P^*\right]^{n^*-2}\left[(a_o/a_o^*)^{\frac{n-2}{2}}-1\right]^{\frac{n^*-2}{n-2}} \quad (6A)$$

The first term in brackets of Eq. (6A) is the minimum time to failure, t_{min}, used to compute proof test diagrams. Therefore Eq. (6A) can be simplified:

$$t/t_{min} = (K_{IC}/K_P^*)^{n^*-2}\left[(a_o/a_o^*)^{\frac{n-2}{2}}-1\right]^{\frac{n^*-2}{n-2}} \quad (7A)$$

By expressing the crack lengths, a_o and a_o^*, of Eq. (7A) in terms of the fracture strength, σ_{IC}, and by using the Weibull equation to relate the strength to the failure probability, the failure time of Eq. (7A) can be expressed in terms of the failure probability. The crack lengths and the strengths are related by the following equation:

$$(a_o/a_o^*)^{1/2} = \sigma_{IC}^*/\sigma_{IC} \quad (8A)$$

since $\sigma_{IC} = K_{IC}/Y\sqrt{a_o}$ and $\sigma_{IC}^* = K_{IC}/Y\sqrt{a_o^*}$. For a given strength distribution, the cumulative probability for failure, P, is related to the strength, σ_{IC}, by the Weibull equation:

$$\ell n\ \ell n\ (1/1-P) = m\ \ell n(\sigma_{IC}/\sigma_o) \quad (9A)$$

where m and σ_o are empirically determined constants. For sufficiently small values of P ($P < 0.1$): $\ell n(1/1-P) = P$. Therefore $P = (\sigma_{IC}/\sigma_o)^m$ and

$P_P = (\sigma^*_{IC}/\sigma_o)^m$, from which the following equation is obtained:

$$P/P_P = (\sigma_{IC}/\sigma^*_{IC})^m \tag{10A}$$

where P_P is equal to the fraction of specimens broken during the proof test. Both P and P_P refer to the initial flaw distribution, the distribution before the proof test. Crack growth alters the initial flaw distribution so that after the proof test the probabilities for failure, P_a, is given by the following equation:

$$P_a = (P - P_P)/(1 - P_P) \tag{11A}$$

If only a small fraction of the components tested are broken, P_P is a small number and to a good approximation:

$$P_a = P - P_P \tag{12A}$$

By substituting Eqs. (12A), (10A), and (8A) into Eq. (7A), an equation relating the failure time, t, to the failure probability, P_a, is obtained:

$$t/t_{min} = (K_{IC}/K^*_P)^{n^*-2}[(1 + P_a/P_P)^{\frac{n-2}{m}} - 1]^{\frac{n^*-2}{n-2}} \tag{13A}$$

For a proof test to be of any value $P_a << P_P$, in which case $(1 + P_a/P_P)^{\frac{n-2}{m}}$

can be expanded by the binomial theorem to give: $(1 + P_a/P_P)^{\frac{n-2}{m}} =$ $1 + (n - 2)\, P_a/mP_P$. Substituting this equation into Eq. (13A) we obtain the following equation relating the failure probability P_a to the failure time, t:

$$P_a = P_P\left(\frac{m}{n-2}\right)\left(K_P^*/K_{IC}\right)^{n-2}\left(t/t_{min}\right)^{\frac{n-2}{n^*-2}} \qquad (14A)$$

By eliminating P_P, Eq. (14A) can be expressed in terms of the Weibull parameters and crack propagation parameters. For small values of P_P: $P_P = \left(\sigma_{IC}^*/\sigma_o\right)^m$, and from the definitions of σ_{IC}^* and K_P^* ($K_{IC} = \sigma_{IC}^* Y\sqrt{a_o^*}$; $K_P^* = \sigma_P Y\sqrt{a_o^*}$): $\sigma_{IC}^* = \sigma_p\left(K_{IC}/K_P^*\right)$. Substituting these two equations into Eq. (14A) we obtain the relationship between the failure probability, P_a, and the Weibull and crack propagation parameters:

$$P_a = \left(\frac{m}{n-2}\right)\left(\sigma_P/\sigma_o\right)^m\left(K_P^*/K_{IC}\right)^{n-m-2}\left(t/t_{min}\right)^{\frac{n-2}{n^*-2}} \qquad (15A)$$

m and σ_o of this equation are determined by a Weibull fit of strength data (measured in an inert environment); n and n^* are crack propagation exponents measured respectively in an inert and active environment; and t_{min} is determined from a proof test diagram.

K_P^* is determined by the proof test conditions. By substituting Eq. (3A) into the definition of K_P^* ($K_P^* = \sigma_p Y\sqrt{a_o^*}$) we obtain the following equation for K_P^*:

$$K_P^* = \sigma_P Y[(A\sigma_P^n Y^n (n - 2)/2)\ (t_P + (t_\ell + t_u)/n + 1)]^{\frac{-1}{n-2}} \qquad (16A)$$

Eq. (16A) can be expressed in a simpler form by defining a crack velocity v_P: $v_P \equiv AK_P^n$, Physically, v_P is the velocity of a crack of length a_o^* if the proof test load is applied instantaneously so that crack growth does not occur during the loading period. After rearranging Eq. (16A) and using the definition of v_P the following equation is obtained:

$$(K_P^*)^2/v_P = [\sigma_P^2 Y^2 (n - 2)/2]\ [t_P + (t_\ell + t_u)/(n + 1)] \qquad (17A)$$

The left-hand side of this equation is determined by the crack propagation data, while the right-hand side is determined by the loading conditions. To determine K_P^*, the right-hand side of Eq. (17A) is evaluated from the proof test conditions,and K_P^* is determined from an experimental plot of K_I^2/v_P versus K_I. This procedure is illustrated for abraded soda lime silicate glass in the main body of the text.

References

1. A. F. Shoemaker, Corning Glass Works, private communication.

2. S. M. Wiederhorn, A. G. Evans and D. E. Roberts, "A Fracture Mechanics Study of the Skylab Windows," in Fracture Mechanics of Ceramics, Vol. II, pp. 829-841, R. C. Bradt, D. P. H. Hasselman, and F. F. Lange, eds., Plenum Press, New York (1974).

3. S. M. Wiederhorn, A. G. Evans, E. R. Fuller and H. Johnson, "Application of Fracture Mechanics to Space Shuttle Windows," to be published in the J. Am. Ceram. Soc., August 1974.

4. A. G. Evans, S. M. Wiederhorn, M. Linzer and E. R. Fuller, "Proof Testing of Porcelain Insulators--And the Application of Acoustic Emission," to be published in the J. Am. Ceram. Soc.

5. W. C. Clark, Jr., Westinghouse Electric Corp., private communication.

6. S. M. Wiederhorn, "Prevention of Failure in Glass by Proof-Testing," J. Am. Ceram. Soc. 56, 227 (1973).

7. A. G. Evans and S. M. Wiederhorn, "Proof Testing of Ceramic Materials--An Analytical Basis for Failure Prediction," NBS Report No. NBSIR 73-147, to be published in Intl. J. Fracture, 1974.

8. A. G. Evans and E. R. Fuller, "Crack Propagation in Ceramic Materials Under Cyclic Loading Conditions," Met. Trans. 5, 27 (1974).

9. A. G. Evans and E. R. Fuller, "Proof Testing--The Effects of Slow Crack Growth," to be published in the J. Am. Ceram. Soc.

10. W. F. Brown and J. E. Srawley, ASTM Special Tech. Publ. No. 410 (1966).

11. A. G. Evans, "Fracture Mechanics Determinations," in Fracture Mechanics of Ceramics, Vol. I, pp. 17-48, R. C. Bradt, D. P. H. Hasselman, and F. F. Lange, eds., Plenum Press, New York (1974).

12. S. M. Wiederhorn, "Subcritical Crack Growth in Ceramics," ibid. Vol. II, pp. 613-646.

13. W. Weibull, "A Statistical Theory of the Strength of Materials," Ingeniörs Vetenskaps Akademien, Handlingar No. 151 (1939).

14. R. W. Davidge, J. R. McLaren and G. Tappin, "Strength-probability-time (SPT) Relationships in Ceramics," J. Mat. Sci. 8, 1699 (1973).

15. C. F. Tiffany and J. N. Masters, pp. 249-77 in Fracture Toughness Testing and Its Applications, ASTM Spec. Tech. Publ. No. 381 (1965).

16. A. G. Evans, "Ceramics for High Performance Applications," this volume.

17. S. M. Wiederhorn, "Influence of Water Vapor on Crack Propagation in Soda-Lime Glass," J. Am. Ceram. Soc. 50, 407 (1967).

18. S. W. Freiman, "The Effect of Organic Alcohols on Crack Propagation in Glass," to be published in the J. Am. Ceram. Soc., August 1974.

19. S. M. Wiederhorn and H. Johnson, "Effect of Electrolyte pH on Crack Propagation in Glass," J. Am. Ceram. Soc. 56, 192 (1973).

20. R. Kossowsky, "The Microstructure of Hot-Pressed Silicon Nitride," J. Mat. Sci. 8, 1603-15 (1973).

21. E. M. Passmore, R. M. Spriggs, and T. Vasilos, "Strength-Grain Size Porosity Relations in Alumina," J. Am. Ceram. Soc. 48, 1-7 (1965).

22. A. G. Evans and S. M. Wiederhorn, "Crack Propagation and Failure Prediction in Silicon Nitride at Elevated Temperatures," J. Mat. Sci., 1974.

23. F. Lange, to be published.

24. A. G. Evans, private communication.

25. S. M. Wiederhorn, H. Johnson, A. M. Diness and A. H. Heuer, "Fracture of Glass in Vacuum," to be published, J. Am. Ceram. Soc., July 1974.

26. S. M. Wiederhorn, "Fracture Surface Energy of Glass," J. Am. Ceram. Soc. 52, 99-105 (1969).

Figure Captions

1. Weibull plot of the strength data for a low expansion glass being considered for the Space Shuttle. The hyperbola gives 95% confidence limits for the best straight-line fit of the data. $m = 6.29$; $\sigma_o = 250\ MN/m^2$. After Wiederhorn, Evans, Fuller and Johnson, reference 3.

2. Statistically based design diagram. For a given value of the failure probability, each line on this diagram relates the failure time to the applied stress. The cross-hatched area gives 95 percent confidence limits for the position of each line.

3. Design diagram based on proof testing. For a given value of the proof test ratio, σ_p/σ_a, each line on this diagram relates the minimum failure time to the applied stress. The numbers over each line give σ_p/σ_a. The probability lines from figure 2 are included here for comparison.

4. Curves to estimate g^{-1} for sinusoidal load. After Evans and Fuller, reference 8.

5. The effect of pH on crack propagation in the low expansion glass being considered for the Space Shuttle. After Wiederhorn, Evans, Fuller and Johnson, reference 3.

6. Proof test diagram comparing power function and exponential function representations of the crack propagation data. The cross, +, marks the lower limit of the crack propagation data. After Wiederhorn, Evans, Fuller and Johnson, reference 3.

7. Strength as a function of loading rate. The brackets represent 95 percent confidence limits for the mean strengths. The solid line is a least squares fit of the strength data. The dashed line was calculated from the crack velocity data for the low expansion glass being considered for the Space Shuttle. After Wiederhorn, Evans, Fuller and Johnson, reference 3.

8. A comparison of the stress rate dependence of the strength predicted from crack velocity data with experimental data obtained by Lange for similar data. After A. G. Evans and S. M. Wiederhorn, reference 22.

9. Dependence of the crack length, a, on the initial crack length, a_o, and crack propagation exponent n. A significant amount of crack growth occurs when $a_o \tilde{-} a_o^*$. For a 5 percent increase in crack length, $a_o = 0.998\ a_o^*$ if $n = 100$; $a_o = 0.90\ a_o^*$ if $n = 20$.

10. Weibull plot of strength data for abraded soda-lime silicate glass. After Evans and Wiederhorn, reference 7.

11. Crack propagation data for soda lime silicate glass in water[12] and in vacuum.[25]

12. Crack propagation data from figure 11 replotted as K_I^2/v versus K_I.

13. Design diagram based on proof testing. Data for soda lime silicate glass. After Evans and Wiederhorn, reference 7.

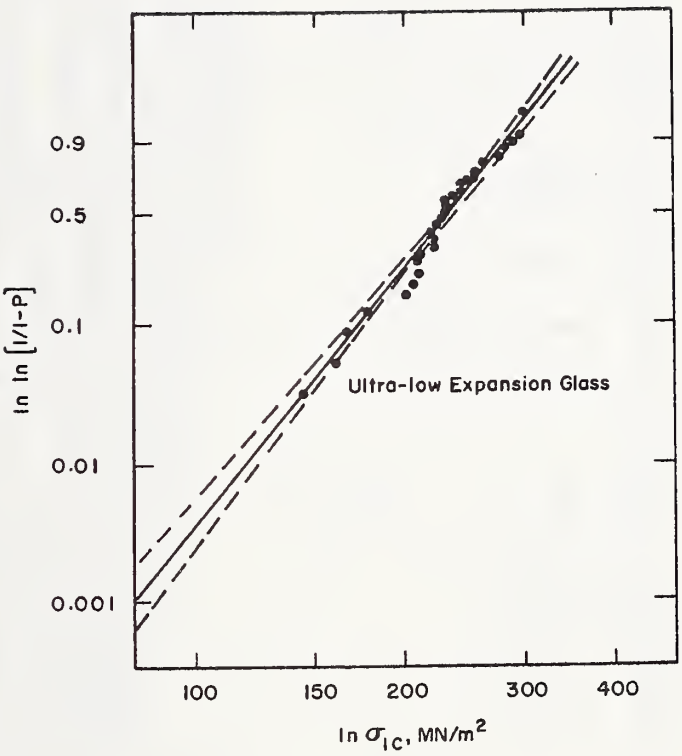

Fig. 1. Weibull plot of the strength data for a low expansion glass being considered for the Space Shuttle. The hyperbola gives 95% confidence limits for the best straight-line fit of the data. $m = 6.29$; $\sigma_o = 250$ MN/m^2. After Wiederhorn, Evans, Fuller and Johnson, reference 3.

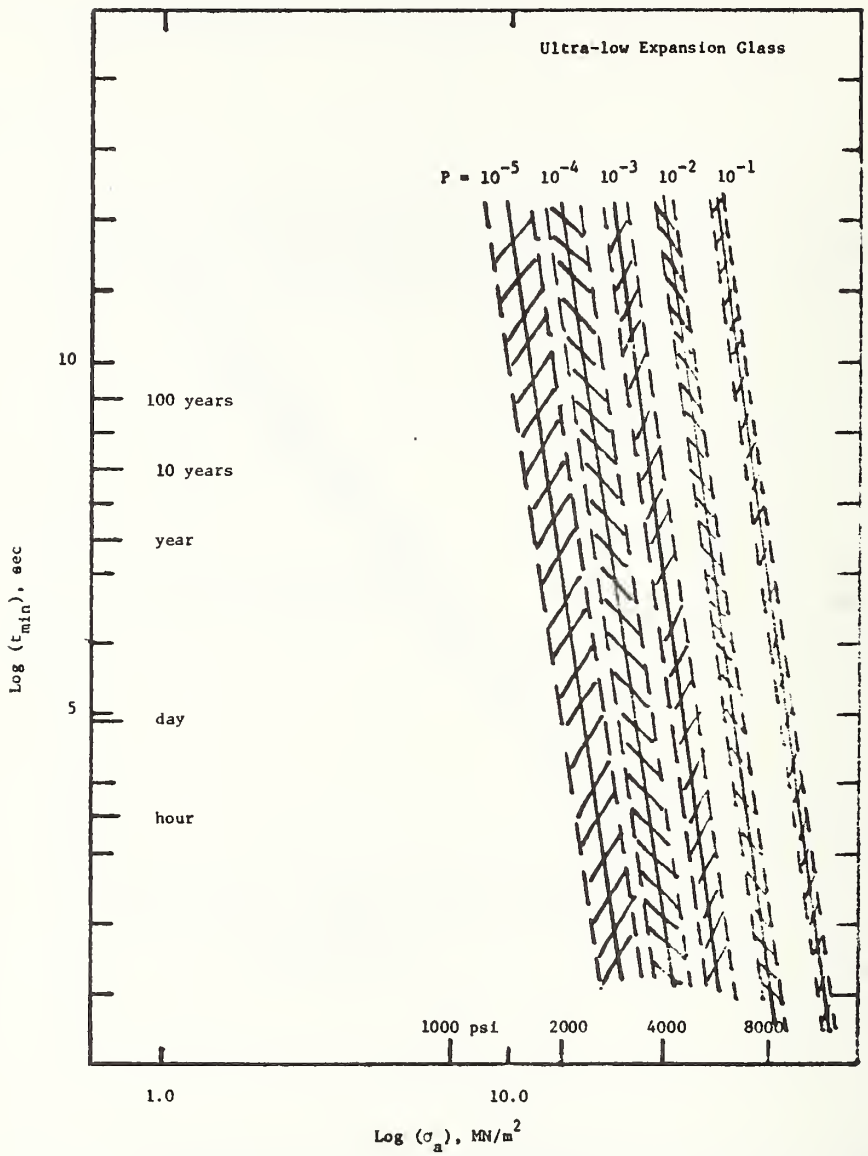

Fig. 2. Statistically based design diagram. For a given value of the failure probability, each line on this diagram relates the failure time to the applied stress. The cross-hatched area gives 95 percent confidence limits for the position of each line.

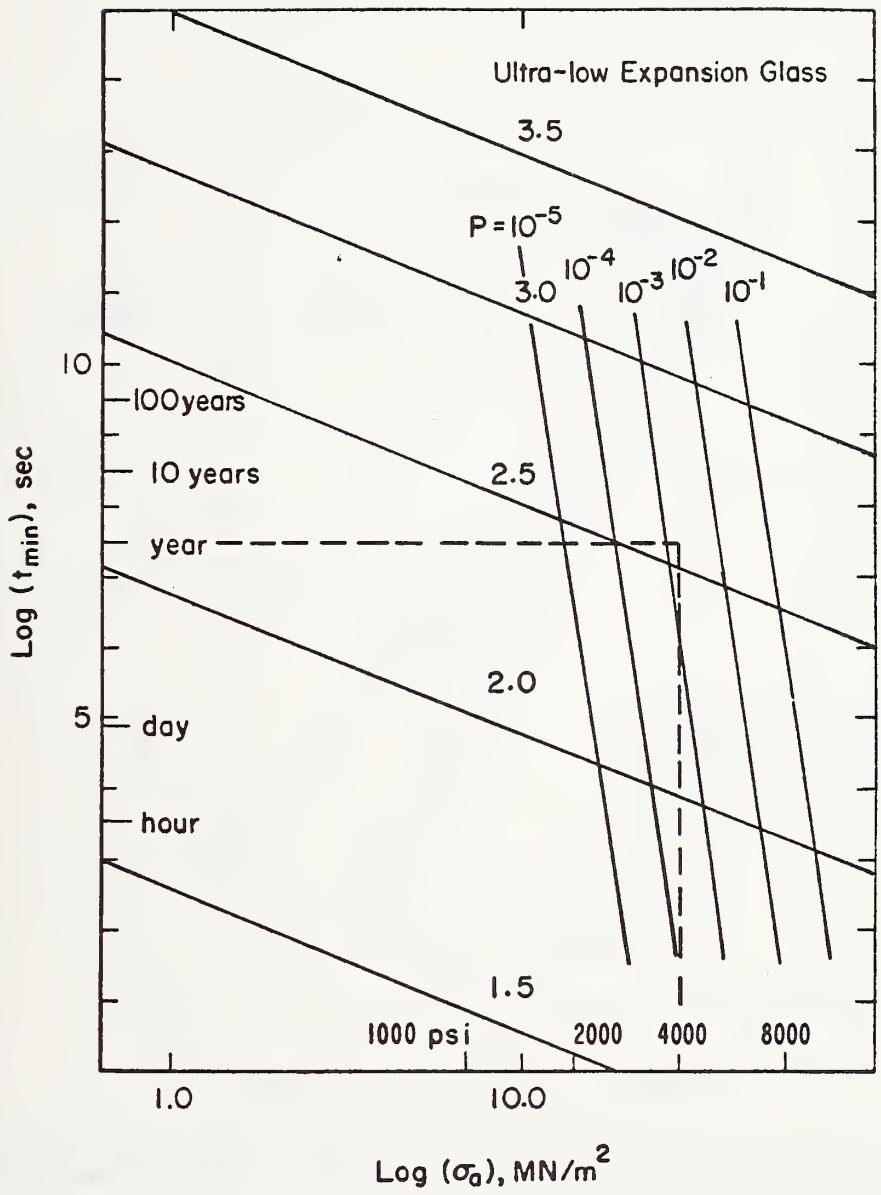

Fig. 3. Design diagram based on proof testing. For a given value of the proof test ratio, σ_p/σ_a, each line on this diagram relates the minimum failure time to the applied stress. The numbers over each line give σ_p/σ_a. The probability lines from figure 2 are included here for comparison.

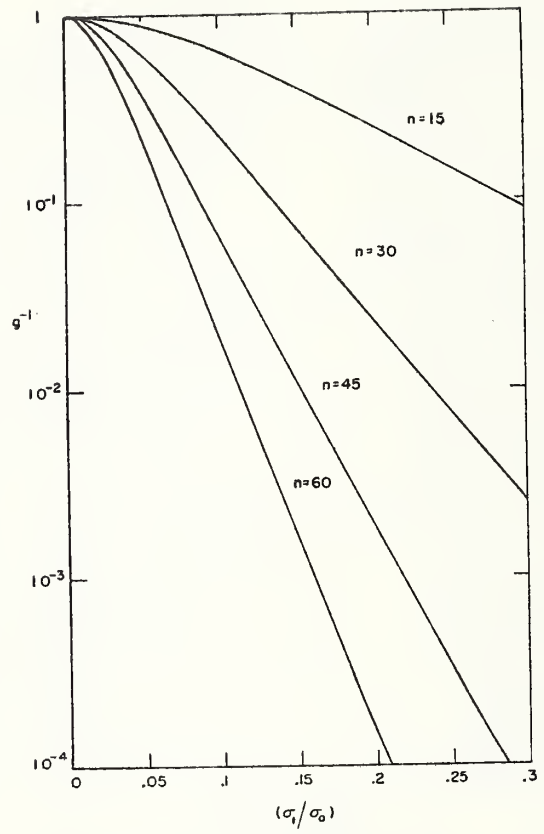

Fig. 4. Curves to estimate g^{-1} for sinusoidal load. After Evans and Fuller, reference 8.

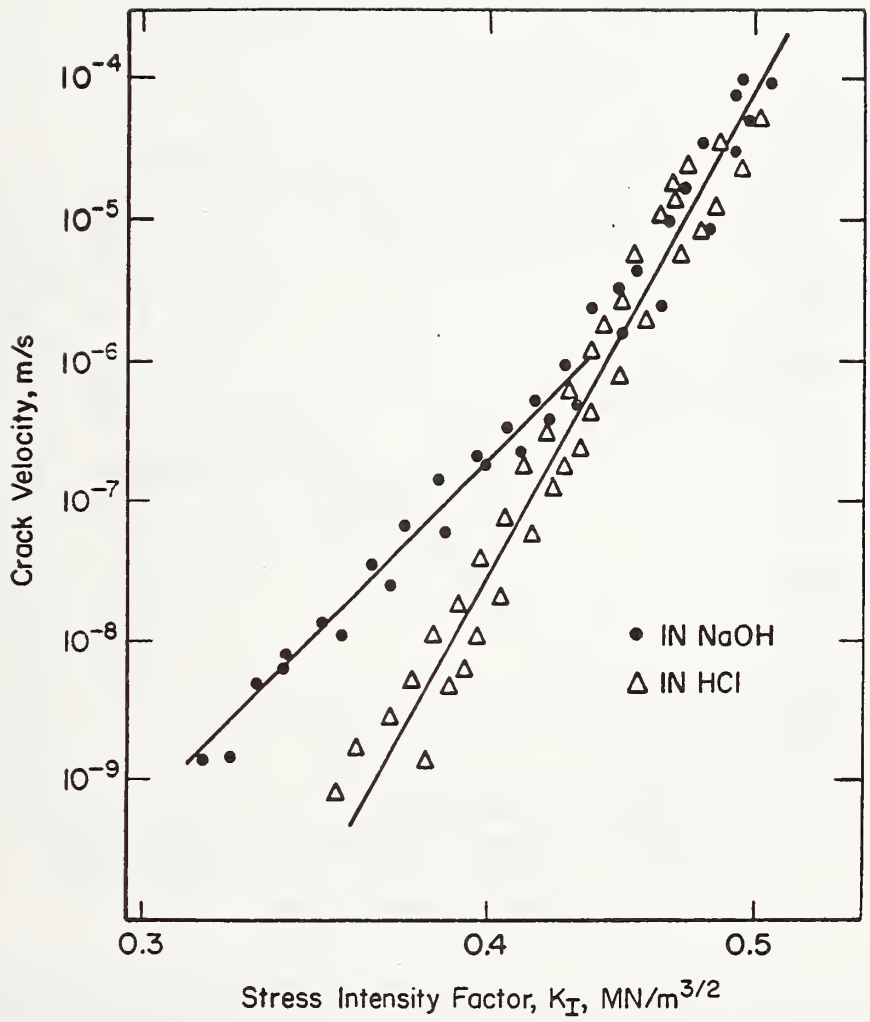

Fig. 5. The effect of pH on crack propagation in the low expansion glass being considered for the Space Shuttle. After Wiederhorn, Evans, Fuller and Johnson, reference 3.

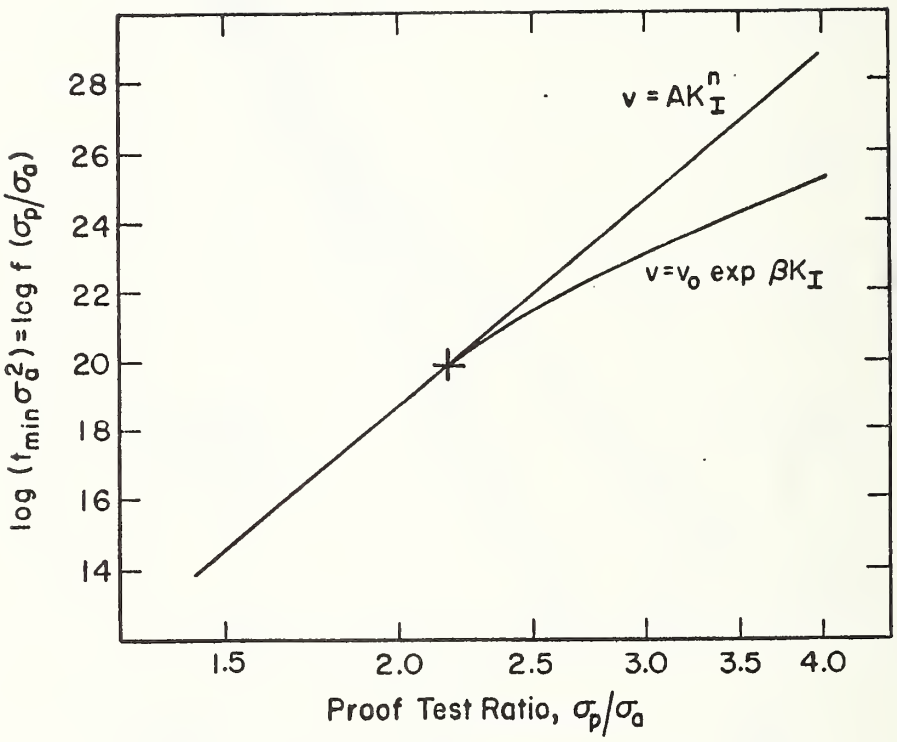

Fig. 6. Proof test diagram comparing power function and exponential function representations of the crack propagation data. The cross, +, marks the lower limit of the crack propagation data. After Wiederhorn, Evans, Fuller and Johnson, reference 3.

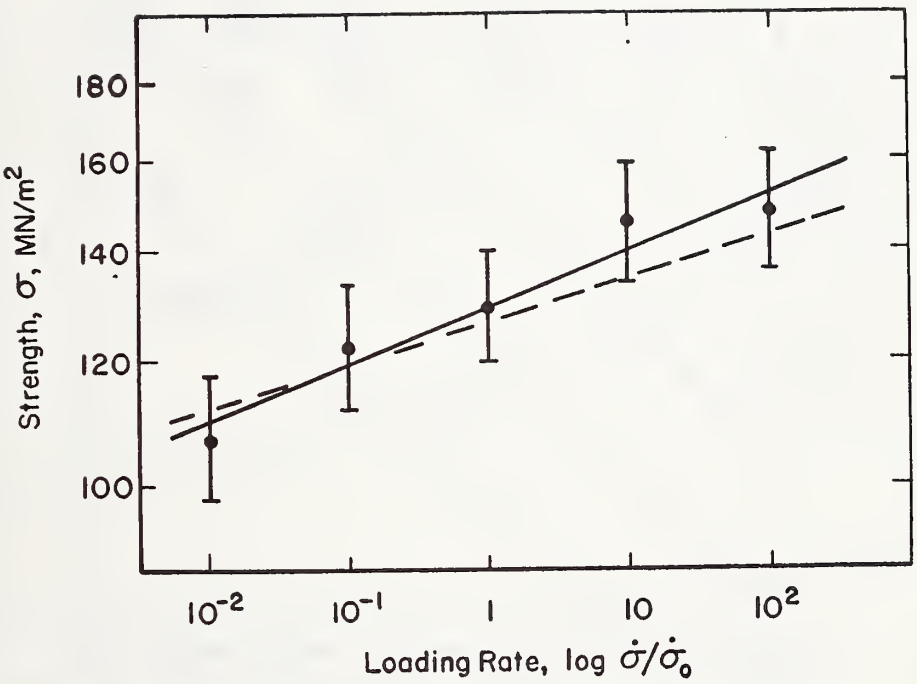

Fig. 7. Strength as a function of loading rate. The brackets represent 95 percent confidence limits for the mean strengths. The solid line is a least squares fit of the strength data. The dashed line was calculated from the crack velocity data for the low expansion glass being considered for the Space Shuttle. After Wiederhorn, Evans, Fuller and Johnson, reference 3.

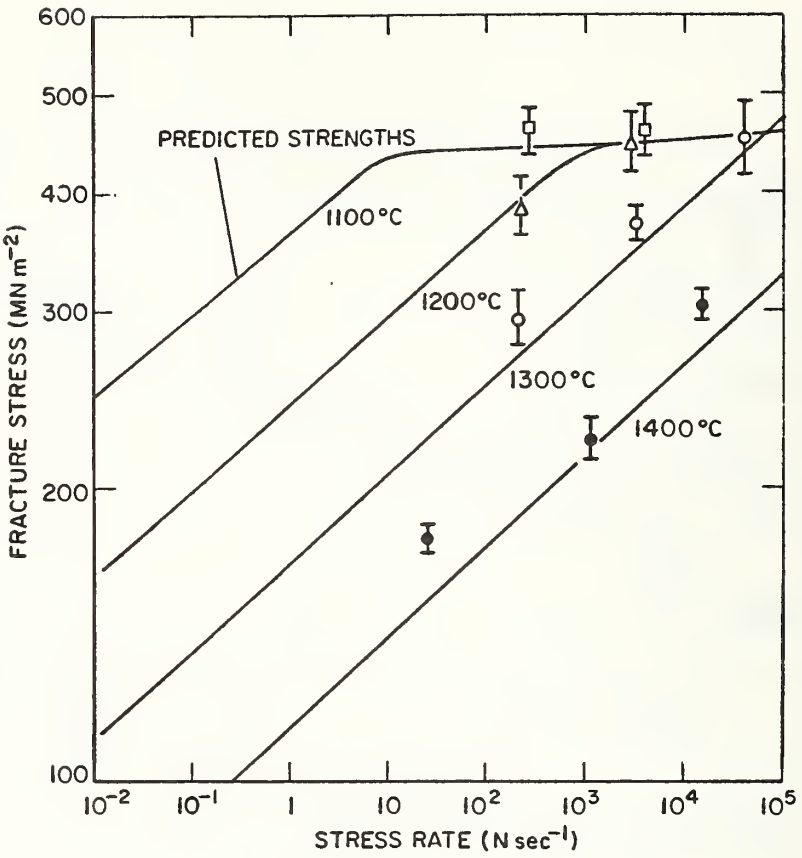

Fig. 8. A comparison of the stress rate dependence of the strength predicted from crack velocity data with experimental data obtained by Lange for similar data. After A. G. Evans and S. M. Wiederhorn, reference 22.

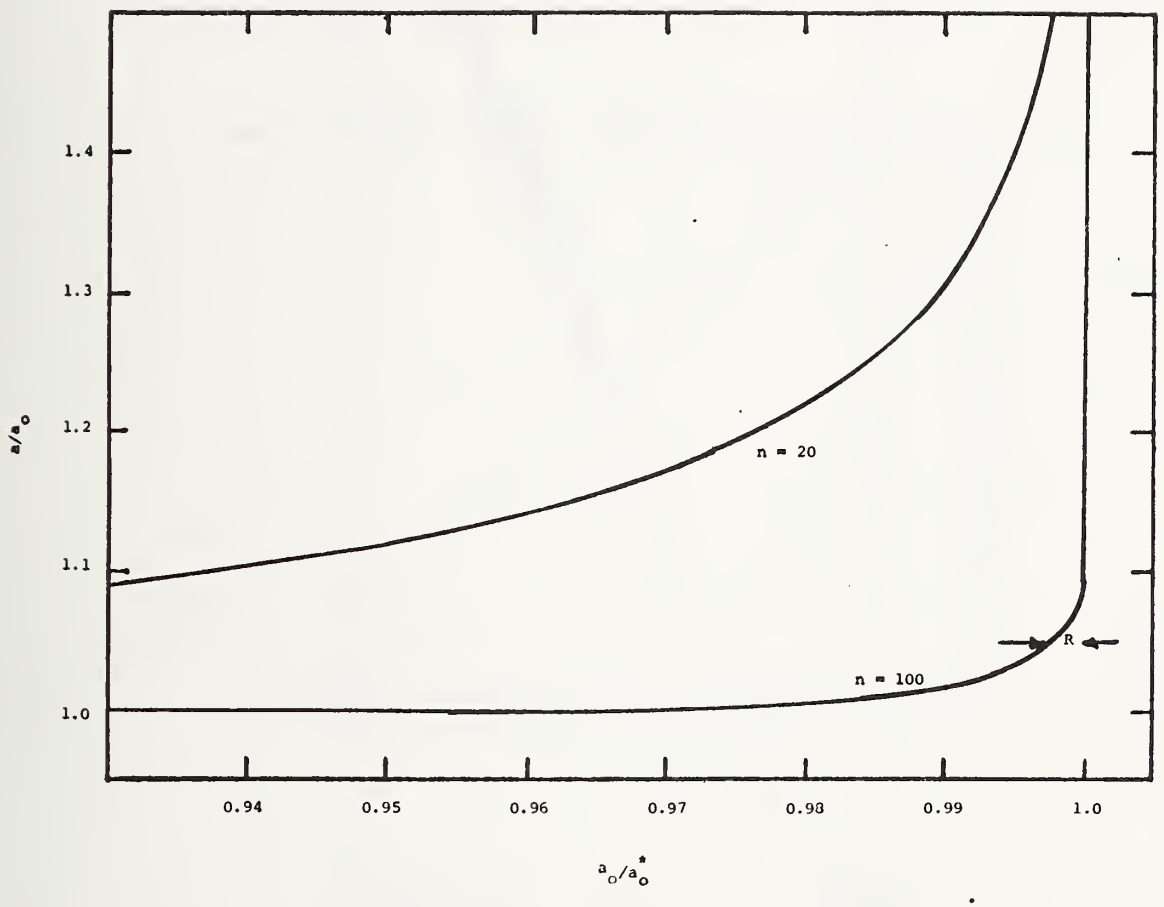

Fig. 9. Dependence of the crack length, a, on the initial crack length, a_o, and crack propagation exponent n. A significant amount of crack growth occurs when $a_o \tilde{=} a_o^*$. For a 5 percent increase in crack length, $a_o = 0.998\ a_o^*$ if n = 100; $a_o = 0.90\ a_o^*$ if n = 20.

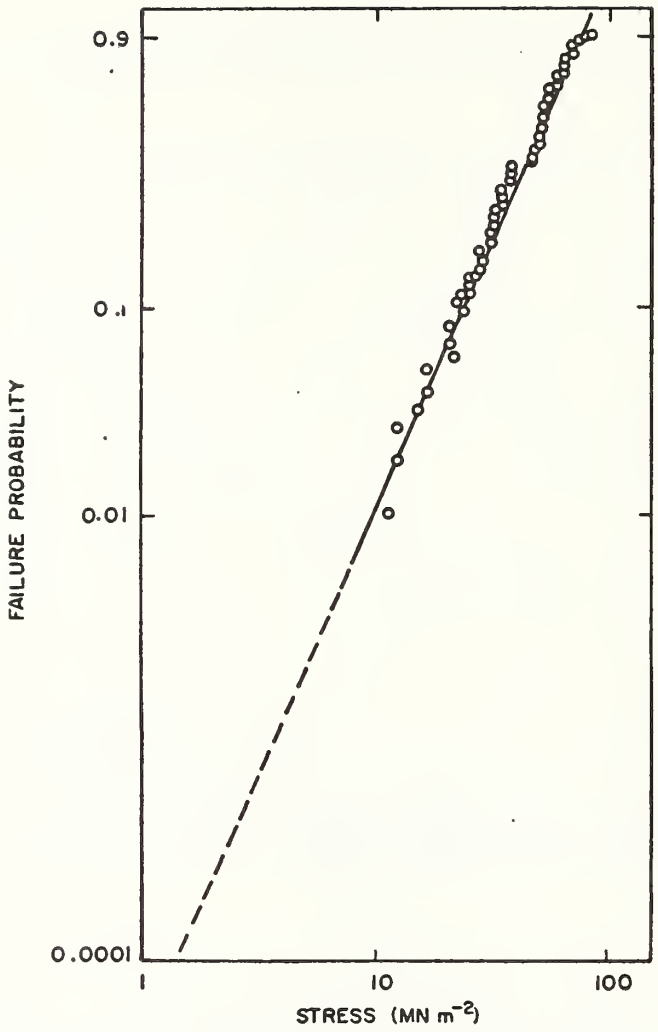

Fig. 10. Weibull plot of strength data for abraded soda-lime silicate glass. After Evans and Wiederhorn, reference 7.

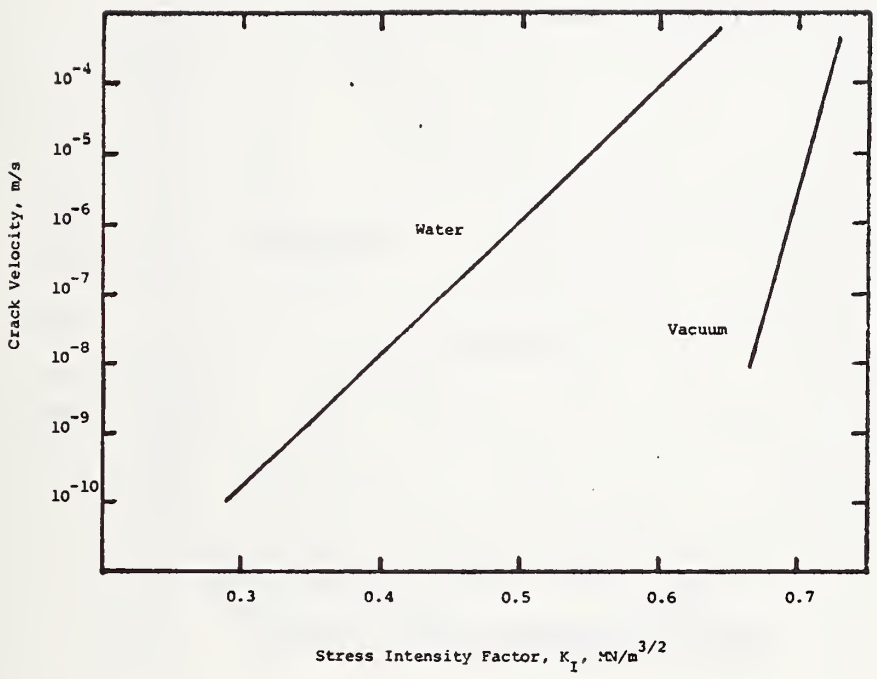

Fig. 11. Crack propagation data for soda lime silicate glass in water[12] and in vacuum.[25]

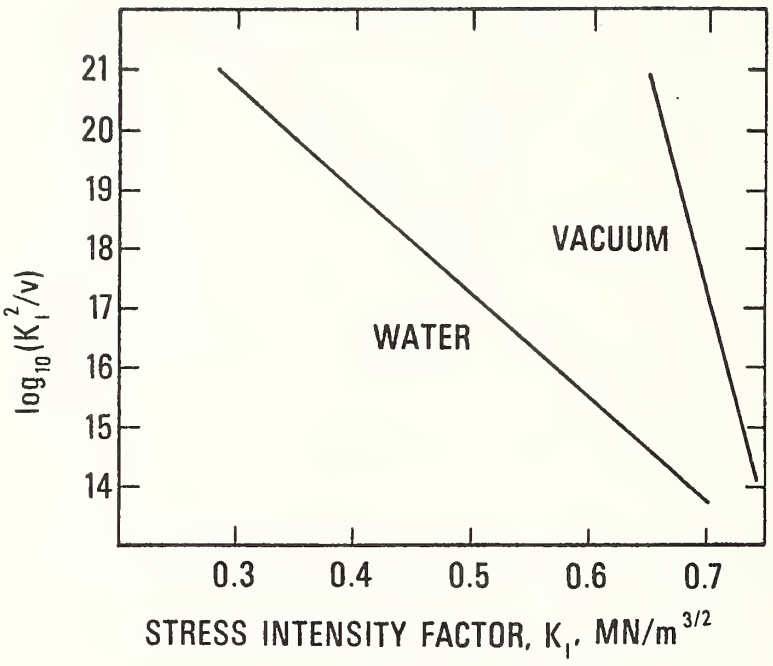

Fig. 12. Crack propagation data from figure 11 replotted as K_I^2/v versus K_I.

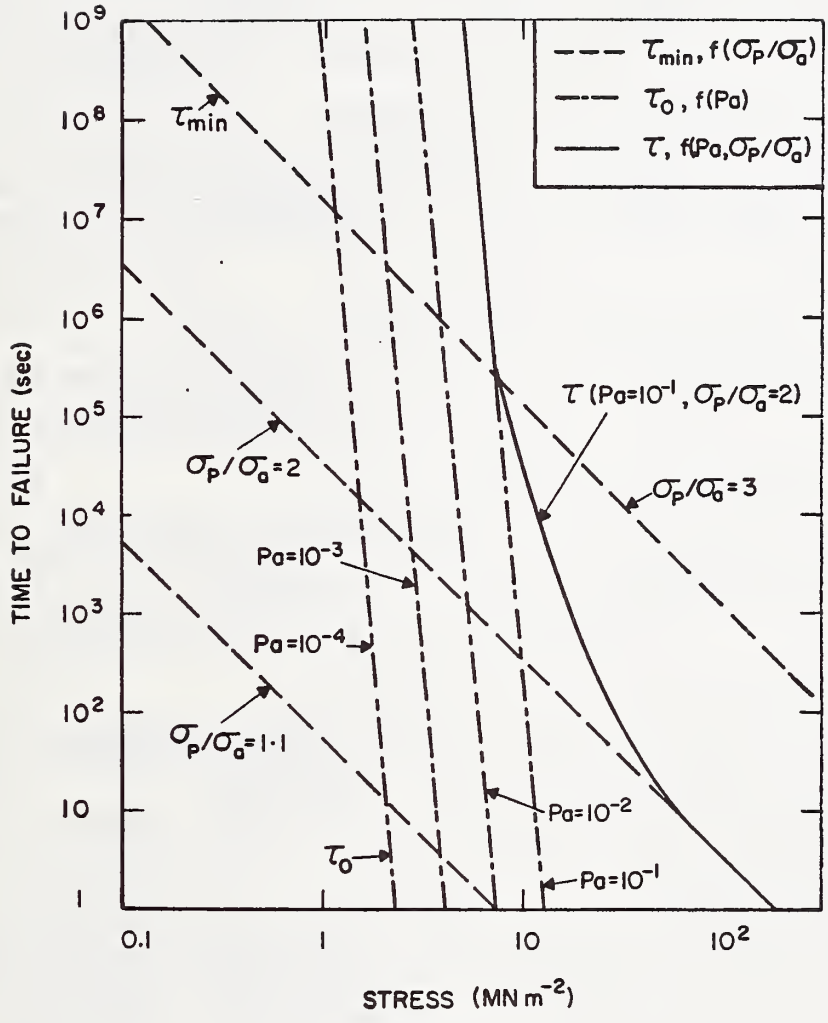

Fig. 13. Design diagram based on proof testing. Data for soda lime silicate glass. After Evans and Wiederhorn, reference 7.

DISTRIBUTION LIST

Organization

Office of Naval Research
Department of the Navy
Attn: Code 471
Arlington, Virginia 22217

Director
Office of Naval Research
Branch Office
495 Summer Street
Boston, Massachusetts 02210

Commanding Officer
Office of Naval Research
New York Area Office
207 West 24th Street
New York, New York 10011

Director
Office of Naval Research
Branch Office
219 South Dearborn Street
Chicago, Illinois 60604

Director
Office of Naval Research
Branch Office
1030 East Green Street
Pasadena, California 91101

Commanding Officer
Office of Naval Research
San Francisco Area Office
50 Fell Street
San Francisco, California 94102

Commanding Officer
Naval Weapons Laboratory
Attn: Research Division
Dahlgren, Virginia 22448

Organization

Director
Naval Research Laboratory
Attn: Technical Information Officer
Code 2000
Washington, D. C. 20390

Director
Naval Research Laboratory
Attn: Technical Information Officer
Code 2020
Washington, D. C. 20390

Director
Naval Research Laboratory
Attn: Technical Information Officer
Code 6000
Washington, D. C. 20390

Director
Naval Research Laboratory
Attn: Technical Information Officer
Code 6100
Washington, D. C. 20390

Director
Naval Research Laboratory
Attn: Technical Information Officer
Code 6300
Washington, D. C. 20390

Director
Naval Research Laboratory
Attn: Technical Information Officer
Code 6400
Washington, D. C. 20390

Director
Naval Research Laboratory
Attn: Library
Code 2029 (ONRL)
Washington, D. C. 20390

Commander
Naval Air Systems Command
Department of the Navy
Attn: Code AIR 320A
Washington, D. C. 20360

Commander
Naval Air Systems Command
Department of the Navy
Attn: Code AIR 5203
Washington, D. C. 20360

Commander
Naval Ordnance Systems Command
Department of the Navy
Attn: Code ORD 033
Washington, D. C. 20360

Commanding Officer
Naval Air Development Center
Aeronautical Materials Div.
Johnsville
Attn: Code MAM
Warminster, Pa. 18974

Commanding Officer
Naval Ordnance Laboratory
Attn: Code 210
White Oak
Silver Spring, Maryland 20910

Commander
Naval Ship Systems Command
Department of the Navy
Attn: Code 0342
Washington, D. C. 20360

Commanding Officer
Naval Civil Engineering Laboratory
Attn: Code L70
Port Hueneme, California 93041

Commander
Naval Ship Engineering Center
Department of the Navy
Attn: Code 6101
Washington, D. C. 20360

Naval Ships R¢D Laboratory
Annapolis Division
Attn: Code A800
Annapolis, Maryland 21402

Commanding Officer
Naval Ships R¢D Center
Attn: Code 747
Washington, D. C. 20007

U. S. Naval Postgraduate School
Attn: Department of Chemistry
and Material Science
Monterey, California 93940

Commander
Naval Weapons Center
Attn: Code 5560
China Lake, California 93555

Commander
Naval Underseas Warfare Center
Pasadena, California 92152

Scientific Advisor
Commandant of the Marine Corps
Attn: Code AX
Washington, D. C. 20380

Commanding Officer
Army Research Office, Durham
Box CM, Duke Station
Attn: Metallurgy ¢ Ceramics Div.
Durham, North Carolina 27706

Office of Scientific Research
Department of the Air Force
Attn: Solid State Div. (SRPS)
Washington, D. C. 20333

Defense Documentation Center
Cameron Station
Alexandria, Virginia 22314

National Bureau of Standards
Attn: Metallurgy Division
Washington, D. C. 20234

National Bureau of Standards
Attn: Inorganic Materials Div.
Washington, D. C. 20234

Atomic Energy Commission
Attn: Metals & Materials Branch
Washington, D. C. 20545

Argonne National Laboratory
Metallurgy Division
P. O. Box 299
Lemont, Illinois 60439

Brookhaven National Laboratory
Technical Information Division
Attn: Research Library
Upton, Long Island, New York 11973

Library
Bldg. 50, Room 134
Lawrence Radiation Laboratory
Berkeley, California 94720

Los Alamos Scientific Laboratory
P. O. Box 1663
Attn: Report Librarian
Los Alamos, New Mexico 87544

Commanding Officer
Army Materials and Mechanics
Research Center
Attn: Res. Programs Office (AMXMR-P)
Watertown, Massachusetts 02172

Director
Metals & Ceramics Division
Oak Ridge National Laboratory
P. O. Box X
Oak Ridge, Tennessee 37830

Commanding Officer
Naval Underwater Systems Center
Newport, Rhode Island 02844

Aerospace Research Laboratories
Wright-Patterson AFB
Building 450
Dayton, Ohio 45433

Defense Metals Information Center
Battelle Memorial Institute
505 King Avenue
Columbus, Ohio 43201

Army Electronics Command
Evans Signal Laboratory
Solid State Devices Branch
c/o Senior Navy Liaison Officer
Fort Monmouth, New Jersey 07703

Commanding General
Department of the Army
Frankford Arsenal
Attn: ORDBA-1320, 64-4
Philadelphia, Pennsylvania 19137

Executive Director
Materials Advisory Board
National Academy of Sciences
2101 Constitution Avenue, N. W.
Washington, D. C. 20418

NASA Headquarters
Attn: Code RRM
Washington, D. C. 20546

Air Force Materials Lab
Wright-Patterson AFB
Attn: MAMC
Dayton, Ohio 45433

Air Force Materials Lab
Wright-Patterson AFB
Attn: MAAM
Dayton, Ohio 45433

Deep Submergence Systems Project
Attn: DSSP-00111
Washington, D. C. 20360

Advanced Research Projects Agency
Attn: Director, Materials Sciences
Washington, D. C. 20301

Army Research Office
Attn: Dr. T. E. Sullivan
3045 Columbia Pike
Arlington, Virginia 22204

Department of the Interior
Bureau of Mines
Attn: Science & Engineering Advisor
Washington, D. C. 20240

Defense Ceramics Information Center
Battelle Memorial Institute
505 King Avenue
Columbus, Ohio 43201

National Aeronautics & Space Adm.
Lewis Research Center
Attn: Librarian
21000 Brookpark Rd.
Cleveland, Ohio 44135

Naval Missile Center
Materials Consultant
Code 3312-1
Point Mugu, California 93041

Commanding Officer
Naval Weapons Center Corona Labs.
Corona, California 91720

Commander
Naval Air Test Center
Weapons Systems Test Div. (Code 01A)
Patuxent River, Maryland 20670

Director
Ordnance Research Laboratory
P. O. Box 30
State College, Pennsylvania 16801

Director
Applied Physics Laboratory
Johns Hopkins University
8621 Georgia Avenue
Silver Spring, Maryland 20901

Director
Applied Physics Laboratory
1013 Northeast Fortieth St.
Seattle, Washington 98105

Materials Sciences Group
Code S130.1
271 Catalina Boulevard
Navy Electronics Laboratory
San Diego, California 92152

Dr. Waldo K. Lyon
Director, Arctic Submarine Laboratory
Code 90, Building 371
Naval Undersea R&D Center
San Diego, California 92132

Dr. R. Nathan Katz
Ceramics Division
U.S. Army Materials & Mechanics
Research Center
Watertown, Mass. 02172

SUPPLEMENTARY DISTRIBUTION LIST

Professor R. Roy
Materials Research Laboratory
Pennsylvania State University
University Park, Pennsylvania 16802

Professor D. H. Whitmore
Department of Metallurgy
Northwestern University
Evanston, Illinois 60201

Professor J. A. Pask
Department of Mineral Technology
University of California
Berkeley, California 94720

Professor D. Turnbull
Div. of Engineering and Applied Science
Harvard University
Pierce Hall
Cambridge, Massachusetts 02100

Dr. T. Vasilos
AVCO Corporation
Research and Advanced Development Div.
201 Lowell Street
Wilmington, Massachusetts 01887

Dr. H. A. Perry
Naval Ordnance Laboratory
Code 230
Silver Spring, Maryland 20910

Dr. Paul Smith
Crystals Branch, Code 6430
Naval Research Laboratory
Washington, D. C. 20390

Dr. A. R. C. Westwood
RIAS Division
Martin-Marietta Corporation
1450 South Rolling Road
Baltimore, Maryland 21227

Prof. M. H. Manghnani
University of Hawaii
Hawaii Institute of Geophysics
2525 Correa Road
Honolulu, Hawaii 96822

Dr. R. H. Doremus
General Electric Corporation
Metallurgy and Ceramics Lab.
Schenectady, New York 12301

Professor G. R. Miller
Department of Ceramic Engineering
University of Utah
Salt Lake City, Utah 84112

Dr. Philip L. Farnsworth
Materials Department
Battelle Northwest
P. O. Box 999
Richland, Washington 99352

Mr. G. H. Haertling
Ceramic Division
Sandia Corporation
Albuquerque, New Mexico 87101

Mr. I. Berman
Army Materials and Mechanics
Research Center
Watertown, Massachusetts 02171

Dr. F. F. Lange
Westinghouse Electric Corporation
Research Laboratories
Pittsburgh, Pennsylvania 15235

Professor H. A. McKinstry
Pennsylvania State University
Materials Research Laboratory
University Park, Pa. 16802

Professor T. A. Litovitz
Physics Department
Catholic University of America
Washington, D. C. 20017

Dr. R. J. Stokes
Honeywell Corporate Research Center
10701 Lyndale Avenue South
Bloomington, Minnesota 55420

Dr. W. Haller
Chief, Inorganic Glass Section
National Bureau of Standards
Washington, D.C. 20234

Dr. Harold Liebowitz
Dean of Engineering
George Washington University
Washington, D. C. 20006

Dr. H. Kirchner
Ceramic Finishing Company
P. O. Box 498
State College, Pennsylvania 16801

Professor A. H. Heuer
Case Western Reserve University
University Circle
Cleveland, Ohio 44106

Dr. D. E. Niesz
Battelle Memorial Institute
505 King Avenue
Columbus, Ohio 43201

Dr. F. A. Kroger
University of Southern California
University Park
Los Angeles, California 90007

Dr. Sheldon M. Wiederhorn
National Bureau of Standards
Inorganic Materials Division
Washington, D.C. 20234

Dr. C. O. Hulse
United Aircraft Research Labs
United Aircraft Corporation
East Hartford, Connecticut 06108

Dr. Stephen Malkin
Department of Mechanical Engineering
University of Texas
Austin, Texas 78712

Prof. H. E. Wilhelm
Department of Mechanical Engineering
Colorado State University
Fort Collins, Colorado 80521

Stanford University
Dept. of Materials Sciences
Stanford, California 94305

Dr. R. K. MacCrone
Department of Materials Engineering
Rensselaer Polytechnic Institute
Troy, New York 12181

Dr. D. C. Mattis
Belfer Graduate School of Science
Yeshiva University
New York, New York 10033

Professor R. B. Williamson
College of Engineering
University of California
Berkeley, California 94720

Professor R. W. Gould
Department of Metallurgical
and Materials Engineering
College of Engineering
University of Florida
Gainesville, Florida 32601

Professor V. S. Stubican
Department of Materials Science
Ceramic Science Section
Pennsylvania State University
University Park, Pennsylvania 16802

Dr. R. C. Anderson
General Electric R and D Center
P. O. Box 8
Schenectady, New York 12301

Dr. Bert Zauderer
MHD Program, Advanced Studies
Room L-9513 - VFSC
General Electric Company
P. O. Box 8555
Philadelphia, Penna. 19101

Prof. C. F. Fisher, Jr.
Department of Mechanical and Aero-
space Engineering
University of Tennessee
Knoxville, Tennessee 37916

NBS-114A (REV 7-73)

U.S. DEPT. OF COMM. BIBLIOGRAPHIC DATA SHEET	1. PUBLICATION OR REPORT NO. NBSIR 74-486	2. Gov't Accession No.	3. Recipient's Accession No.

4. TITLE AND SUBTITLE

. Reliability, Life Prediction and Proof Testing of Ceramics

5. Publication Date

6. Performing Organization Code

7. AUTHOR(S)
S. M. Wiederhorn

8. Performing Organ. Report No.
NBSIR 74-486

9. PERFORMING ORGANIZATION NAME AND ADDRESS

NATIONAL BUREAU OF STANDARDS
DEPARTMENT OF COMMERCE
WASHINGTON, D.C. 20234

10. Project/Task/Work Unit No.
3130453

11. Contract/Grant No.
NR-032-517

12. Sponsoring Organization Name and Complete Address *(Street, City, State, ZIP)*
Department of the Navy
Office of Naval Research
Code 471, 800 N. Quincy Street
Arlington, Virginia 22217

13. Type of Report & Period Covered
Interim
7-1-73 thru 6-30-74

14. Sponsoring Agency Code

15. SUPPLEMENTARY NOTES

16. ABSTRACT *(A 200-word or less factual summary of most significant information. If document includes a significant bibliography or literature survey, mention it here.)*

A critical review is presented of the use of proof testing as a design method for assuring the reliability of structural components. The advantage of proof testing over the statistical approach used for design lies in the insensitivity of the proof testing method to the detailed history of handling or processing of structural components. Methods are presented for developing and using proof test diagrams to assure component lifetime after proof testing. Procedures of proof testing and precautions that must be followed during proof testing are discussed. Provided these precautions are followed, proof testing offers a general method for assuring the reliability of structural components under stress.

17. KEY WORDS *(six to twelve entries; alphabetical order; capitalize only the first letter of the first key word unless a proper name; separated by semicolons)*
Ceramics; crack propagation; delayed failure; fracture; proof testing; Weibull analysis.

18. AVAILABILITY [X] Unlimited

[ ] For Official Distribution. Do Not Release to NTIS

[ ] Order From Sup. of Doc., U.S. Government Printing Office Washington, D.C. 20402, SD Cat. No. C13

[ ] Order From National Technical Information Service (NTIS) Springfield, Virginia 22151

19. SECURITY CLASS (THIS REPORT)
UNCLASSIFIED

21. NO. OF PAGES
60

20. SECURITY CLASS (THIS PAGE)
UNCLASSIFIED

22. Price